RhoA activation during polarization and cytokinesis of the early *Caenorhabditis elegans* embryo is differentially dependent on NOP-1 and CYK-4

Yu Chung Tse[a,*], Michael Werner[a,*,†], Katrina M. Longhini[a], Jean-Claude Labbe[b,‡], Bob Goldstein[b], and Michael Glotzer[a]

[a]Department of Molecular Genetics and Cell Biology, University of Chicago, Chicago, IL 60637; [b]Department of Biology, University of North Carolina at Chapel Hill, Chapel Hill, NC 27599

ABSTRACT **The GTPase RhoA is a central regulator of cellular contractility in a wide variety of biological processes. During these events, RhoA is activated by guanine nucleotide exchange factors (GEFs). These molecules are highly regulated to ensure that RhoA activation occurs at the proper time and place. During cytokinesis, RhoA is activated by the RhoGEF ECT-2. In human cells, ECT-2 activity requires its association with CYK-4, which is a component of the centralspindlin complex. In contrast, in early *Caenorhabditis elegans* embryos, not all ECT-2–dependent functions require CYK-4. In this study, we identify a novel protein, NOP-1, that functions in parallel with CYK-4 to promote RhoA activation. We use mutations in *nop-1* and *cyk-4* to dissect cytokinesis and cell polarization. NOP-1 makes a significant, albeit largely redundant, contribution to cytokinesis. In contrast, NOP-1 is required for the preponderance of RhoA activation during the establishment phase of polarization.**

Monitoring Editor
Jeffrey D. Hardin
University of Wisconsin

Received: Apr 6, 2012
Revised: Jul 12, 2012
Accepted: Aug 14, 2012

INTRODUCTION

The small GTPase RhoA is a central regulator of cellular contractility. When activated by exchanging its bound GDP cofactor for GTP, this molecular switch activates formins and Rho kinase, which stimulates polymerization of unbranched actin filaments and promotes assembly and activation of minifilaments of nonmuscle myosin II, respectively (for a review, see Piekny *et al.*, 2005). RhoA and its effectors constitute a contractile module that impacts diverse biological processes. Two such processes, cell polarization and cytokinesis, have been extensively analyzed in the early *Caenorhabditis elegans* embryo (Munro and Bowerman, 2009). These processes share a number of molecular, genetic, and cytological similarities. Notably, cortical contractility, which is critical for both processes, is dependent on RhoA activation by the guanine nucleotide exchange factor (GEF) ECT-2 (Dechant and Glotzer, 2003; Zonies *et al.*, 2010).

Although cytokinesis and cell polarization share requirements for ECT-2, RhoA, and their downstream effectors, the mechanisms that trigger ECT-2 activation during these processes appear to be molecularly distinct. During cytokinesis, but not polarization, ECT-2 activation involves extensive interactions with CYK-4, a component of the centralspindlin complex that contains a Rho-family GTPase-activating protein (GAP) domain. The N-terminus of ECT-2 contains tandem BRCA1 C-Terminal (BRCT) domains that bind to phosphorylated CYK-4 and contribute to its activation (Burkard *et al.*, 2009; Wolfe *et al.*, 2009). The BRCT domains also bind to and inhibit the catalytic C-terminus (Kim *et al.*, 2005), suggesting that CYK-4 binding promotes relief from autoinhibition. The integrity of the GAP domain of CYK-4—although

This article was published online ahead of print in MBoC in Press (http://www.molbiolcell.org/cgi/doi/10.1091/mbc.E12-04-0268) on August 23, 2012.

*These authors contributed equally to this work.

Present addresses: †Feinberg School of Medicine, Northwestern University, Chicago, IL 60611; ‡Department of Pathology and Cell Biology, Université de Montréal, Montréal, PQ H3C 3J7, Canada.

Address correspondence to: Michael Glotzer (mglotzer@uchicago.edu).

Abbreviations used: AH, conserved region; BRCT, BRCA1 C-Terminal domain; CCD, charge-coupled device; DIC, differential interference contrast; dsRNA, double-stranded RNA; GAP, GTPase-activating protein; GEF, guanine nucleotide exchange factor; GFP, green fluorescent protein; NEBD, nuclear envelope breakdown; NGM, nematode growth medium; PH, pleckstrin homology; RNAi, RNA interference.

Supplemental Material can be found at:
http://www.molbiolcell.org/content/suppl/2012/08/20/mbc.E12-04-0268.DC1.html

not necessarily its catalytic activity—is also required for full activation of RhoA during cytokinesis in a variety of experimental systems (Yamada *et al.*, 2006; Canman *et al.*, 2008; Loria *et al.*, 2012). However, loss-of-function mutations in CYK-4 that cripple its ability to promote RhoA activation in cytokinesis appear to have little effect on RhoA activation during embryo polarization (Canman *et al.*, 2008; Loria *et al.*, 2012).

Polarization of the early *C. elegans* embryo involves an initial establishment phase that is followed by a mechanistically distinct maintenance phase (Cuenca *et al.*, 2003). The establishment phase is initiated by fertilization, which activates global cortical contractility. The sperm-provided centrosome and its associated astral microtubules locally suppress contractility near the posterior pole (Cowan and Hyman, 2004; Tsai and Ahringer, 2007). The resulting nonuniform contractility induces anterior-directed cortical flow and concentration of numerous proteins, including myosin and the polarity factors PAR-3, PAR-6, and PKC-3, to the anterior of the embryo (Munro *et al.*, 2004). This flow is accompanied by a transient, cytokinetic-like furrow called the pseudocleavage furrow. Concomitant with this flow, posterior PAR proteins, such as PAR-1 and PAR-2, are recruited to the posterior cortex and prevent the return of the anterior PARs to the posterior cortex (Cuenca *et al.*, 2003; Munro *et al.*, 2004). A second, microtubule-dependent pathway can direct cortical PAR-2 recruitment when cortical flows are eliminated (Motegi *et al.*, 2011). During the maintenance phase, anteriorly localized CDC-42 promotes polarized activation of myosin via myotonic dystrophy kinase–related Cdc42-binding kinase and activation of ARP2/3-dependent actin polymerization (Gotta *et al.*, 2001; Kay and Hunter, 2001; Kumfer *et al.*, 2010). Symmetry-breaking polarization is robust; perturbations that result in clear molecular phenotypes can be tolerated, but combinations of these perturbations can block polarization (Zonies *et al.*, 2010).

Cleavage furrow ingression in early *C. elegans* embryos is mediated by two distinct pathways that can be distinguished by their dependence on the central spindle (Dechant and Glotzer, 2003; Bringmann and Hyman, 2005). Central spindle–independent, also known as aster-directed, furrowing resembles the pseudocleavage furrow in that both invariably undergo furrow regression. Additionally, a number of perturbations have been described that preferentially impair central spindle–independent furrowing; these perturbations also prevent pseudocleavage furrow formation (Werner and Glotzer, 2008). One such case is that of embryos depleted of anillin (ANI-1). ANI-1 promotes the organization of cortical myosin into large foci and its polarization along the anterior–posterior axis (Maddox *et al.*, 2005; Tse *et al.*, 2011). Interestingly, whereas cleavage furrows ingress asymmetrically in control embryos, they ingress symmetrically in embryos depleted of either ANI-1 or the septins (Maddox *et al.*, 2007). No other factors are known that regulate the asymmetry of furrow ingression.

A maternal effect mutation, *nop-1(it142)*, has been described that abrogates cortical contractility during the establishment phase of polarization without dramatically affecting cytokinesis (Rose *et al.*, 1995). In fact, homozygous *nop-1* mutant animals are viable and fertile, although ~20% of these embryos fail to hatch. *nop-1* mutant embryos also fail to form an anterior actin cap, indicating a defect in organization or function of the cytoskeleton. However, the molecular nature of NOP-1 has not been established. We report the molecular identification of NOP-1 and show that this protein promotes RhoA-dependent processes during the establishment phase of polarization and during cytokinesis. NOP-1 is required for the majority of RhoA activation during polarization, whereas it acts in parallel to the centralspindlin-dependent pathway for RhoA activation during cytokinesis.

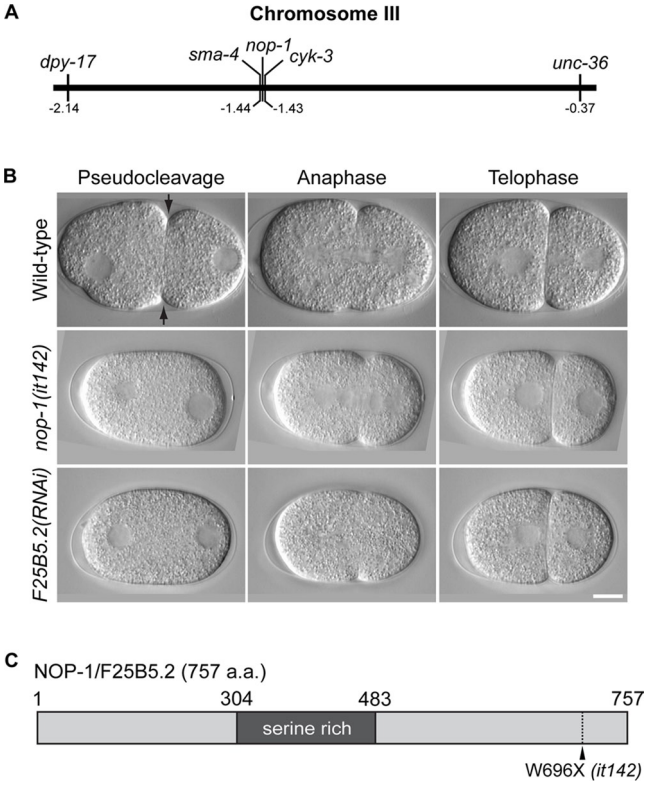

FIGURE 1: Identification of NOP-1. (A) *nop-1* maps to −1.43 on chromosome III, between *sma-4* and *cyk-3*. (B) Images from a time-lapse sequence of the first division of wild-type, *nop-1(it142)*, and *nop-1(RNAi)* embryos at the indicated cell cycle phases. Wild-type embryos form pseudocleavage furrows (black arrows), whereas pseudocleavage is absent in *nop-1(it142)* and *nop-1(RNAi)* embryos. Scale bar: 10 µm. (C) Schematic depicting the domain structure of NOP-1. The dotted line indicates the premature stop codon found in *nop-1(it142)*.

RESULTS

Molecular identification of NOP-1

nop-1 was originally mapped to a position on chromosome III between *dpy-17* and unc-32 (Rose *et al.*, 1995). Further mapping experiments revealed that the mutation is located in the 0.01 cM region between *sma-4* and *cyk-3* on chromosome III (Figure 1A). To identify *nop-1*, we depleted all the genes in this region by RNA interference (RNAi) and filmed early embryos using Nomarski microscopy. RNAi depletion of one gene, F25B5.2, blocked formation of the pseudocleavage furrow and phenocopied the *nop-1(it142)* mutation (Figure 1B, Figure 1 Movie S1). Furthermore, in *nop-1(it142)*, we identified a premature stop codon near the end of the predicted open reading frame, at amino acid 696 (Figure 1C). Embryonic lethality occurs in similar fractions of *nop-1(it142)*, F25B5.2(RNAi), and *nop-1(it142)*;F25B5.2(RNAi) embryos (~27%). These results, together with the rescue data below, indicate that *nop-1* is encoded by the F25B5.2 gene and that *nop-1(it142)* is a strong loss-of-function mutation, perhaps even a null.

NOP-1 is a 757-residue, serine-rich (16.8%) protein lacking recognizable domains or motifs. Orthologues of NOP-1 can be readily identified in the related nematodes *Caenorhabditis briggsae*, *Caenorhabditis japonicus*, *Caenorhabditis brennerei*, and *Caenorhabditis remanei* (Supplemental Figure S1). However, despite extensive efforts, we were unable to identify orthologues in other species.

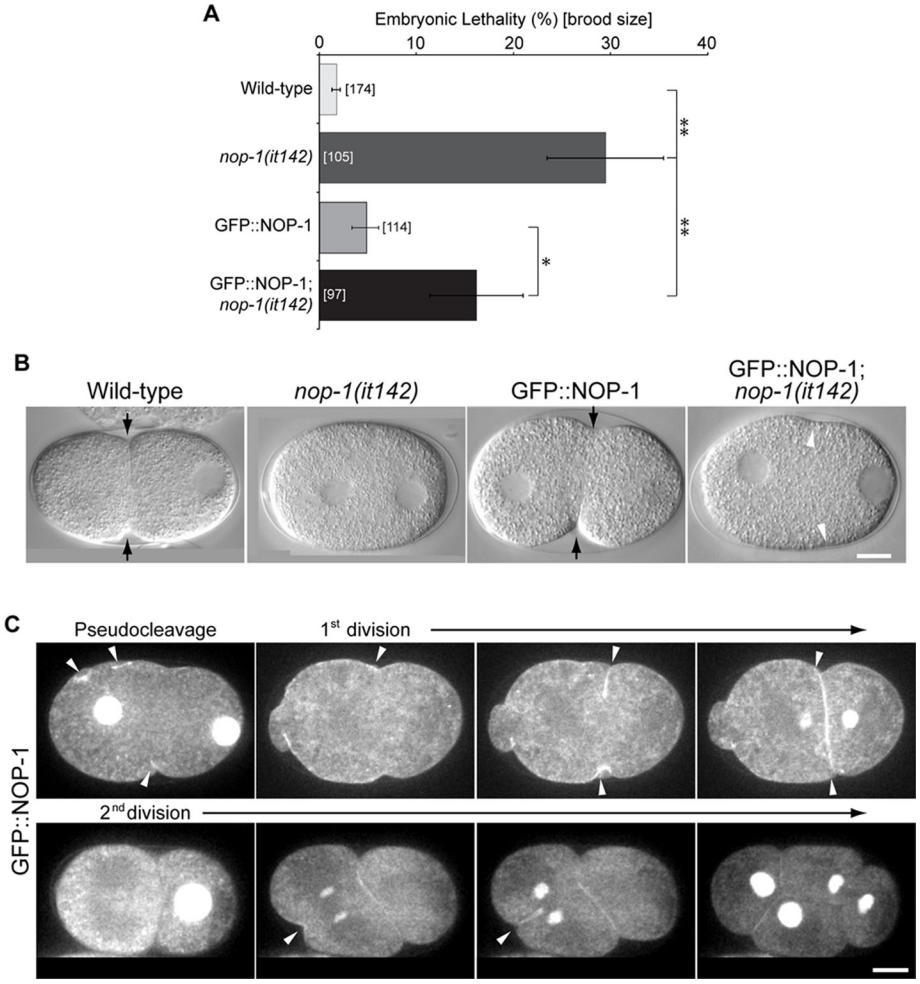

FIGURE 2: GFP::NOP-1 partially rescues *nop-1(it142)* and localizes to the nucleus and cleavage furrow. (A) Embryonic lethality and average brood size in wild-type, *nop-1(it142)*, GFP::NOP-1, and GFP::NOP-1;*nop-1(it142)* worms (error bars represent ± SEM, *, $p < 0.05$; **, $p < 0.01$). (B) Selected images from time-lapse sequences of wild-type, *nop-1(it142)*, GFP::NOP-1, and *nop-1(it142)*;GFP::NOP-1 embryos. Black arrows indicate pseudocleavage furrows, and white arrowheads indicate partially rescued pseudocleavage furrows in GFP::NOP-1;*nop-1(it142)*. (C) Selected confocal images from time-lapse sequences of embryos expressing GFP::NOP-1. White arrowheads indicate the recruitment of GFP::NOP-1 in the cleavage furrow. Scale bars: 10 µm.

Localization of NOP-1

To determine the subcellular localization of NOP-1 in *C. elegans* embryos, we inserted a green fluorescent protein (GFP)-tagged NOP-1 transgene controlled by the germ line–active PIE-1 regulatory elements into the *C. elegans* genome using MosSCI (Frøkjaer-Jensen *et al.*, 2008). GFP::NOP-1 does not have a strong dominant effect on embryonic viability or progression of cytokinesis, although the brood size is slightly reduced (Figure 2, A and B). GFP::NOP-1 partially rescued both the pseudocleavage defect and the lethality resulting from the *nop-1(it142)* mutation (Figure 2, A and B, Figure 2 Movie S1), confirming the gene identification. We imaged embryos expressing GFP::NOP-1 from pseudocleavage to completion of cytokinesis using time-lapse confocal microscopy. GFP::NOP-1 dramatically concentrates in interphase nuclei. In addition to a significant cytoplasmic pool, a distinct cortical localization can be detected, particularly at ingressing pseudocleavage and cleavage furrows (Figure 2C, Figure 2 Movie S2). Similar results were obtained when the localization of endogenous NOP-1 was assessed with an antibody raised against a peptide from the C-terminus of NOP-1 (Supplemental Figure S2).

NOP-1 promotes cortical recruitment of RhoA effectors

To determine how NOP-1 regulates pseudocleavage, we investigated the dynamic localization of mediators of cortical contractility. We recorded time-lapse images of control and *nop-1(it142)* embryos expressing NMY-2::GFP, GFP::ANI-1 and GFP::Utrophin from the time of pronuclear migration to telophase using spinning-disk confocal microscopy (Figure 3). As reported previously, in control embryos, NMY-2::GFP forms large patches in the anterior half of embryos during pseudocleavage (Munro *et al.*, 2004). These patches then dissociate, and smaller punctae accumulate in the anterior region and form an anterior cap of myosin during prometaphase. On anaphase onset, this anterior cap dissipates and NMY-2::GFP reaccumulates, forming large patches primarily at the equatorial region and near the anterior pole (Figure 3A, Figure 3 Movie S1). The pattern of myosin recruitment was dramatically different in *nop-1(it142)* embryos. Large NMY-2::GFP patches were absent from *nop-1(it142)* embryos during pseudocleavage (Figure 3A and Supplemental Figure S3). As the pronucleus migrates, small NMY-2::GFP foci are evenly distributed throughout the entire cortex, and cortical flow is greatly attenuated. The anterior cap of smaller myosin punctae forms during prometaphase, although its boundary extends more posteriorly than in control embryos (see following section). This cap then dissipates as in control embryos, and discrete, small NMY-2::GFP foci reaccumulate specifically in the equatorial region and induce furrow ingression (Figure 3A, Figure 3 Movie S1). Thus the large myosin patches that appear during pseudocleavage and anaphase in control embryos are NOP-1–dependent.

RhoA activation also triggers the cortical accumulation of the cytokinetic scaffold protein anillin, which largely colocalizes with myosin in control embryos (Maddox *et al.*, 2005). In anillin-depleted embryos, myosin accumulates in the cortex, but the patches are dramatically smaller. In contrast, cortical anillin accumulates normally in myosin-depleted embryos (Maddox *et al.*, 2005; Tse *et al.*, 2011). Therefore cortical recruitment of anillin and myosin are partially independent markers for RhoA activation. We therefore investigated whether inactivation of NOP-1 also affects anillin. Anillin patches are absent from *nop-1(it142)* embryos; only small cortical foci are observed during pseudocleavage and in the equatorial region during cytokinesis (Figures 3B and S3, Figure 3 Movie S1). Quantitative analysis reveals that NOP-1 promotes cortical recruitment of both anillin and myosin, as well as the accumulation of equatorial cortical actin (Supplemental Figure S3).

Examination of fixed embryos indicates that *nop-1(it142)* embryos are defective in cortical actin accumulation (Rose *et al.*, 1995). To gain more insight into this phenotype, we characterized the dynamic patterning of actin in live embryos using GFP::Utrophin, a probe derived

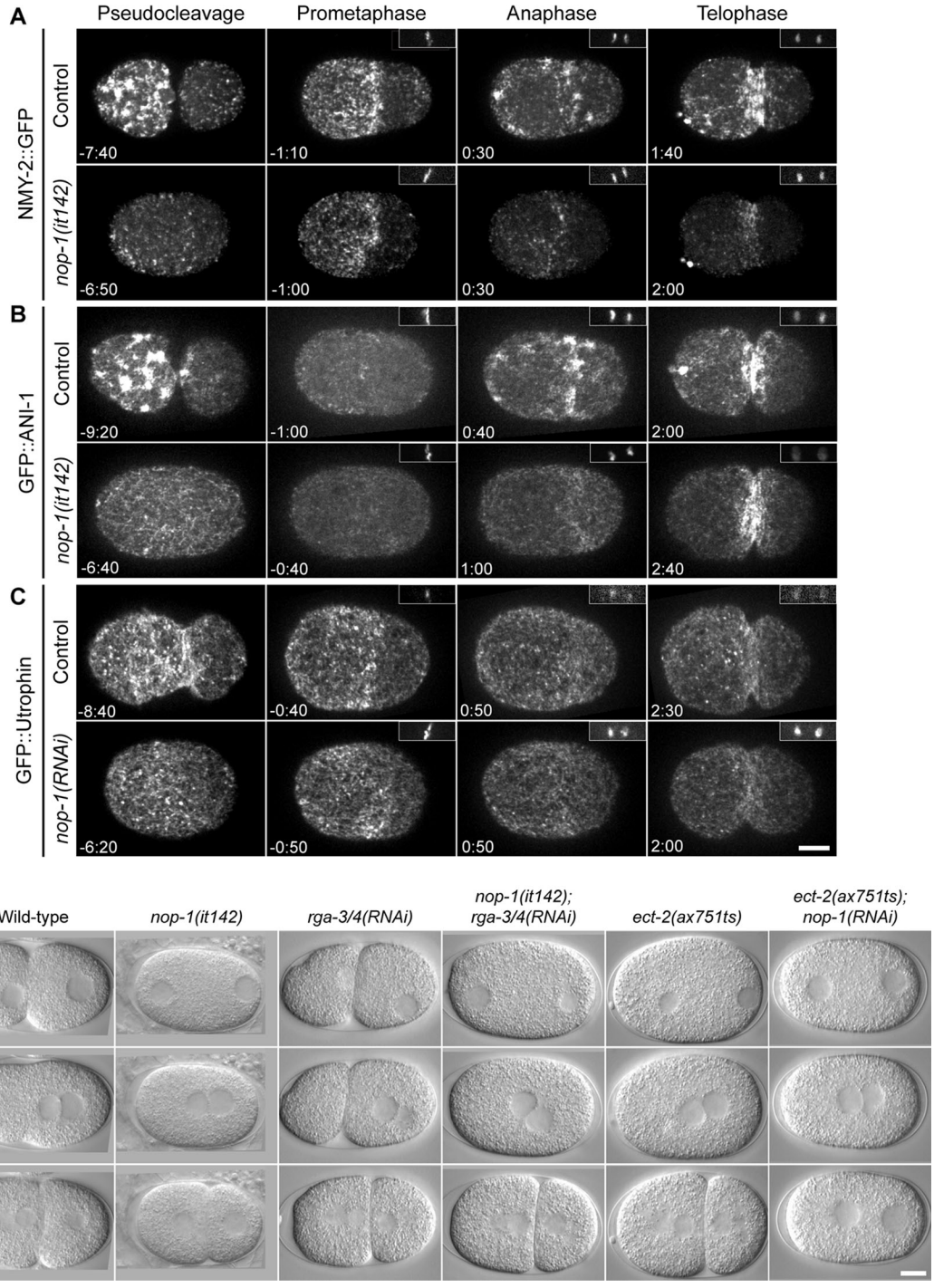

FIGURE 3: NOP-1 mediates cortical recruitment of Rho effectors and promotes Rho activation. (A–C) Selected confocal images from time-lapse sequences of control and *nop-1(it142)* or *nop-1(RNAi)* embryos expressing (A) NMY-2::GFP, (B) GFP::ANI-1, and (C) GFP::Utrophin at the indicated times relative to anaphase onset. Insets (right, top) show the chromatin as detected with mCherry::HIS. All images are projections of five planes spanning 2 µm. (D) Selected DIC images from time-lapse sequences of wild-type, *nop-1(it142)*, *rga-3/4(RNAi)*, *nop-1(it142);rga-3/4(RNAi)*, *ect-2(ax751ts)*, and *ect-2(ax751ts);nop-1(RNAi)* at the indicated stages. Scale bars: 10 µm.

from the F-actin–binding calponin homology domain of utrophin (Burkel *et al.*, 2007). In control embryos, cortical filamentous actin and actin puncta form in the anterior half of embryos during pseudocleavage. Like myosin, actin filaments become enriched in the anterior half of the embryo and form an anterior cap during prometaphase. The cap then disperses and actin filaments reappear at the site of cleavage (Figure 3C, Supplemental Figure S3, and Figure 3 Movie S1). The overall dynamic behavior of actin filaments in *nop-1(it142)* embryos is similar to controls. However, the actin cap during pseudocleavage is attenuated. In addition, accumulation of actin filaments at the equatorial region during cytokinesis is slightly delayed in NOP-1–depleted embryos. Thus NOP-1 promotes the cortical recruitment of anillin and myosin during both pseudocleavage and cytokinesis and promotes the accumulation of actin at furrowing regions.

NOP-1 functions upstream of ECT-2

Contractile behavior during pseudocleavage and cytokinesis in the early embryo is dependent on the RhoGEF ECT-2 (Jenkins *et al.*, 2006; Motegi and Sugimoto, 2006; Schonegg and Hyman, 2006; Werner *et al.*, 2007). The primary RhoGAPs that antagonize ECT-2 are RGA-3/4, two highly related RhoGAPs (Schmutz *et al.*, 2007; Schonegg *et al.*, 2007). Depletion of RGA-3/4 leads to increased cortical contractility during polarization and cytokinesis (Figure 3D). The observations shown thus far indicate that NOP-1 promotes the accumulation of active RhoA. In principle, NOP-1 could perform this function by inhibiting RGA-3/4. If NOP-1 functioned upstream of RGA-3/4, then co-inactivation of NOP-1 and RGA-3/4 should phenocopy RGA-3/4 depletion. We acquired time-lapse differential interference contrast (DIC) images of control and *nop-1(it142)* embryos depleted of RGA-3/4. Cortical contractions are enhanced and pseudocleavage persists until the pronuclei centrates in *rga-3/4(RNAi)* embryos (Figure 3D, Figure 3 Movie S2). In contrast, cortical ruffling and pseudocleavage are absent in *nop-1(it142);rga-3/4(RNAi)* embryos (Figure 3D, Figure 3 Movie S2), indicating that NOP-1 is epistatic to RGA-3/4 and does not inhibit it. As a second test for residual RhoA activity in early *nop-1* embryos, we used another mutant that causes hypercontractility, *rfl-1(or198ts)*. Depletion of NOP-1 in *rfl-1(or198ts)* embryos also causes a cessation of cortical contractility during pseudocleavage (Supplemental Figure S4).

Further evidence that NOP-1 contributes to cytokinetic furrowing arises from analysis of *ect-2(ax751ts);nop-1(RNAi)* embryos. In *ect-2(ax751ts)* embryos, cortical ruffling and pseudocleavage are absent (Figure 3D) yet cytokinesis proceeds to completion in most embryos at the semipermissive temperature (Zonies *et al.*, 2010), resembling the phenotype of *nop-1(it142)* embryos (Figures 1B and 6A). Whereas both *ect-2(ax751ts)* and *nop-1(RNAi)* embryos are able to complete cytokinesis efficiently, doubly compromised embryos do not exhibit cytokinetic furrowing (Figure 3D, Figure 3 Movie S2). This genetic interaction is consistent with a model in which NOP-1 and ECT-2 act in a common pathway or in parallel to activate RhoA.

If NOP-1 and ECT-2 functioned in parallel, contractility would be predicted to persist in embryos in which either protein is strongly depleted. During pseudocleavage, this is not the case, contractility is absent in both single mutants (Figure 3D). Furthermore, during cytokinesis, strong depletion of ECT-2 is sufficient to abrogate cortical contractility. Indeed, cortical accumulation of anillin during anaphase is reduced to near background levels by strongly depleting ECT-2 (Supplemental Figure S5). Depletion of ECT-2 in *nop-1(it142)* embryos results in a marginally stronger effect, although it is difficult to exclude the possibility that this slight difference depends on residual ECT-2 activity (Supplemental Figure S5). Thus, during cytokinesis, NOP-1 requires ECT-2 to generate contractility, but not vice versa. These data suggest that NOP-1 acts upstream of ECT-2.

NOP-1 mediates aster-induced furrowing

Two independent pathways contribute to furrow formation in the early *C. elegans* embryo: central spindle–directed furrowing and aster-directed furrowing (Dechant and Glotzer, 2003; Bringmann and Hyman, 2005). The molecular mechanism of aster-induced furrowing during cytokinesis shares numerous similarities with pseudocleavage during polarity establishment. The genetic requirements of the two processes are similar and, in each case, a furrow forms at the border between an anterior region enriched in cortical myosin and a posterior region depleted of this motor protein (Werner *et al.*, 2007; Afshar *et al.*, 2010). We therefore asked whether NOP-1 regulates aster-directed furrowing during cytokinesis. Depletion of the centralspindlin subunit ZEN-4 inactivates central spindle-induced furrowing; all the residual furrowing is aster-dependent (Werner *et al.*, 2007). In wild-type and *nop-1(it142)* embryos, furrows ingress during anaphase and cytokinesis completes in most embryos (Figure 4A). In *zen-4(RNAi)* embryos, furrows ingress and then regress (Figure 4A). However, cleavage furrow formation is completely blocked in *nop-1(it142);zen-4(RNAi)* doubly compromised embryos (Figure 4A, Figure 4 Movie S1). To further determine whether NOP-1 is essential for the aster-induced pathway, we spatially separated the furrows that result from these two pathways in the same embryo by depleting the microtubule-associated protein ZYG-9 (Werner *et al.*, 2007). Inactivation of ZYG-9 results in shorter microtubules and the spindle becomes mispositioned at the posterior pole. ZYG-9–depleted embryos form central spindle-dependent and aster-induced furrows in the posterior and the anterior regions of the zygote, respectively (Werner *et al.*, 2007). The formation of anterior furrow is blocked in both *nop-1(it142);zyg-9(RNAi)* and *nop-1(it142);zyg-9(b244ts)* embryos (Figure 4B). Interestingly, the posterior furrow is perturbed in a subset of *nop-1(it142);zyg-9(RNAi)* embryos (40%) and *nop-1(it142);zyg-9(b244ts)* embryos (25%). NOP-1 is thus critical for aster-directed furrowing and makes a subtle, but detectable, contribution to central spindle-dependent furrowing.

Control of cytokinetic furrowing by independent RhoA activators

Recent work has demonstrated that CYK-4 is required for activating RhoA during central spindle–directed furrowing. An allele of *cyk-4*, *or749ts*, contains a substitution mutation in the GAP domain; this is a separation-of-function allele in which central spindle assembly is normal, but there is a dramatic reduction in the cortical accumulation of myosin, F-actin, and anillin and central spindle–directed furrowing is absent (Canman *et al.*, 2008; Loria *et al.*, 2012). The previous experiment suggests that NOP-1 also promotes RhoA activation, although it primarily contributes to aster–directed furrowing. These results suggest that NOP-1 and CYK-4 could be partially redundant activators of ECT-2 that are collectively responsible for ECT-2 activation. This model predicts that *nop-1;cyk-4(or749ts)* embryos would fail to recruit RhoA effectors upon anaphase onset and would fail to form cleavage furrows altogether. We imaged *nop-1(RNAi);cyk-4(or749ts)* embryos and found that the doubly compromised embryos indeed fail to form cleavage furrows upon anaphase onset (Figure 4A and Figure 4 Movie S1). In addition, cortical recruitment of myosin and anillin at the equatorial region upon anaphase onset are attenuated in *cyk-4(or749ts);nop-1(RNAi)* embryos (Figure 4, C and D); F-actin accumulation is also modestly reduced (Figure 4E).

NOP-1 promotes RhoA activation

To confirm that the cortical recruitment of RhoA effectors reliably reflects RhoA activity, we developed a RhoA biosensor. This sensor consists of GFP fused to the C-terminal portion of *C. elegans* anillin, which contain its conserved region (AH) and pleckstrin homology (PH) domain. It lacks the N-terminal myosin- and actin-binding domains but retains its RhoA-binding domain. This sensor is similar to one used in human cells that colocalizes with the cortical pool of active RhoA (Piekny and Glotzer, 2008). This truncated anillin does not dominantly interfere with anillin function; pseudocleavage occurs normally, and cytokinetic furrowing is asymmetric. This sensor was validated in *C. elegans* by assaying its cortical abundance in control, ECT-2–depleted and RGA-3/4–depleted embryos. In control embryos, GFP::AHPH is cortically recruited during pseudocleavage and

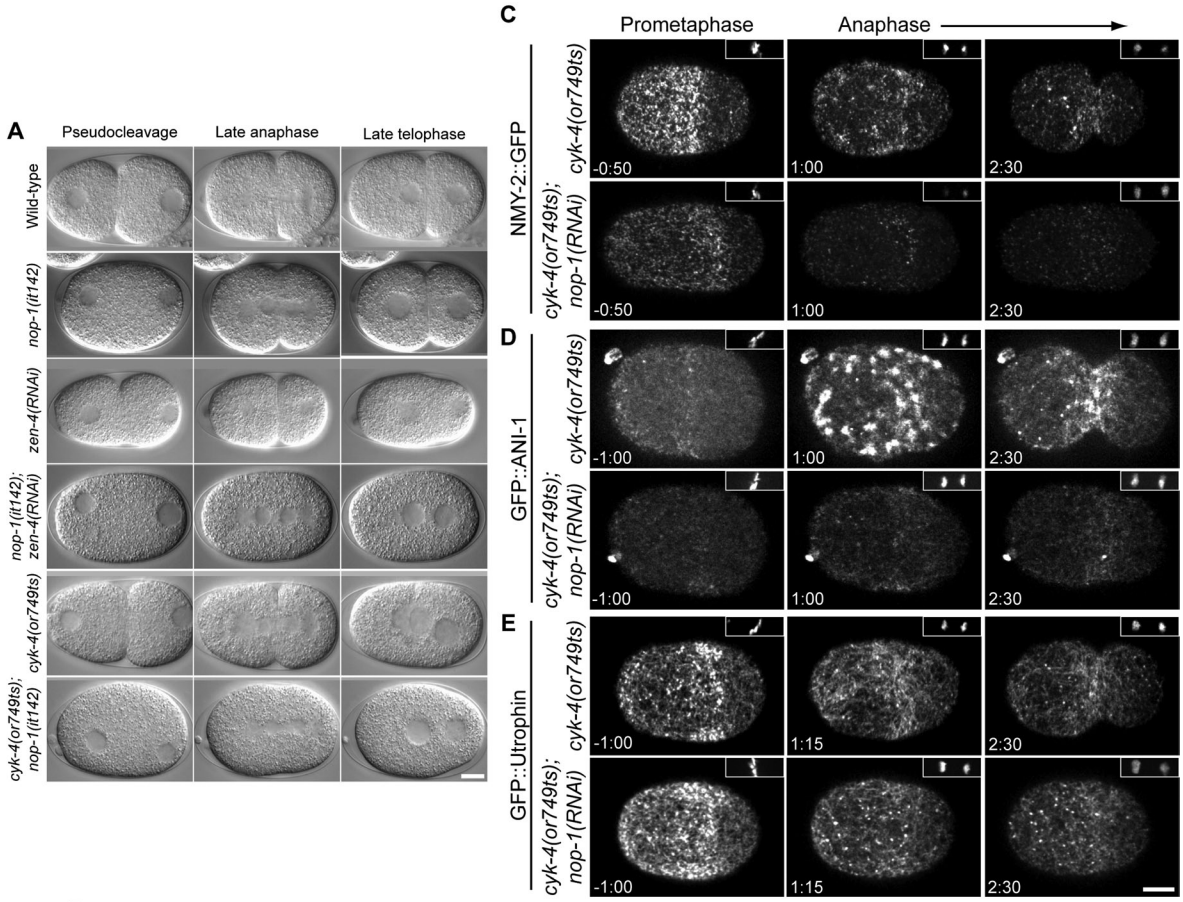

B

	N	No furrow (%)	Anterior furrow (%)	Posterior furrow (%)	Anterior and Posterior furrow (%)
zyg-9(RNAi)	8	0	0	0	100
zyg-9(b244ts)	8	0	0	0	100
nop-1(it142); zyg-9(RNAi)	9	44.4	0	55.6	0
nop-1(it142); zyg-9(b244ts)	8	25	0	75	0

FIGURE 4: NOP-1 regulates aster-induced cleavage furrows. (A) Selected images from time-lapse sequences of wild-type, *nop-1(it142)*, *zen-4(RNAi)*, *nop-1(it142); zen-4(RNAi)*, *cyk-4(or749ts)*, and *cyk-4(or749ts);nop-1(RNAi)* embryos at the indicated cell cycle phases. (B) The number of ZYG-9–depleted embryos with anterior and posterior furrows in control and NOP-1–depleted embryos. (C–E) Selected confocal images from time-lapse sequences of *cyk-4(or749ts)* and *cyk-4(or749ts);nop-1(RNAi)* embryos expressing NMY-2::GFP (C), GFP::ANI-1 (D), and GFP::Utrophin (E) at the indicated times relative to anaphase onset. Insets (top, right) show the chromatin as detected by mCherry::HIS. Scale bars: 10 μm.

cytokinesis, a pattern that resembles that of GFP:anillin (Figure 5, A and B). The cortical abundance of this reporter in the equatorial region declines when ECT-2 is depleted (Supplemental Figure S6, A–C) and increases when RGA-3/4 are depleted (Supplemental Figure S6, B and C). Cortical recruitment of the biosensor does not require downstream effectors of RhoA. Moderate depletion of NMY-2 causes a slight increase in sensor recruitment (Supplemental Figure S6, B and C), stronger depletion results in a more dramatic increase (Supplemental Figure S6A). ANI-1 depletion causes a stronger increase in biosensor recruitment (Supplemental Figure S6, B and C). These results suggest that RhoA may be coupled through feedback regulation to downstream processes. Alternatively, or in addition, there may be competition of the sensor with endogenous ANI-1. These results indicate that GFP::AHPH is a reliable indicator of RhoA activation.

The RhoA biosensor was used to assess whether loss-of-function mutations in NOP-1 and/or CYK-4 result in reduced RhoA activation. During polarization, GFP::AHPH accumulation at the cell cortex is NOP-1–dependent (Figure 5A). During cytokinesis, cortical GFP::AHPH in the furrow region is reduced in both *nop-1(it142)* embryos and *cyk-4(or749ts)* embryos (Figure 5, B and C). However, in each case there is residual accumulation of GFP::AHPH. In *nop-1(RNAi)* embryos, GFP::AHPH accumulation is moderately reduced, whereas in *cyk-4(or749ts)* embryos, GFP::AHPH is dramatically reduced, although it remains detectable (Figure 5, B and C). In *nop-1(RNAi);cyk-4(or749ts)* embryos, no cortical GFP::AHPH was observed, confirming that NOP-1 and CYK-4 act in parallel to activate RhoA (Figure 5, B and C, and Supplemental Figure S6A).

NOP-1 can modulate asymmetric cleavage furrow ingression

Because the cortical accumulation of myosin, anillin, and actin are altered in NOP-1–depleted embryos, we investigated whether these molecular defects affect ingression of the cleavage furrow. Initiation of cleavage furrow ingression is slightly delayed in NOP-1–depleted embryos (Figure 6A), but furrowing completes with kinetics similar to those of control embryos (Figure 6, B and C). Given that both anillin and NOP-1 primarily promote aster-directed furrowing, we examined the behavior of embryos in which both of these factors are inactivated. Both individual perturbations abrogate pseudocleavage furrowing, but neither prevents cytokinesis. Anillin-depleted embryos have an additional phenotype in which furrow formation occurs symmetrically (Maddox *et al.*, 2007; Figure 6, A and B). In contrast, cleavage furrows of *nop-1(it142)* embryos ingress asymmetrically, similar to control embryos (Figure 6, A and B). Asymmetric furrowing in *nop-1(it142)* embryos could result from central spindle–directed accumulation of anillin (compare Figures 3B and 4D). Surprisingly, we found that furrow formation is asymmetric in *ani-1(RNAi);nop-1(it142)* embryos (Figure 6, A and B). The vast majority of these embryos also exhibit hyperaccumulation of PH:GFP at the furrow tips (Figure 6A). These results reveal the existence of an ANI-1–independent mechanism for generating asymmetrically ingressing cleavage furrows.

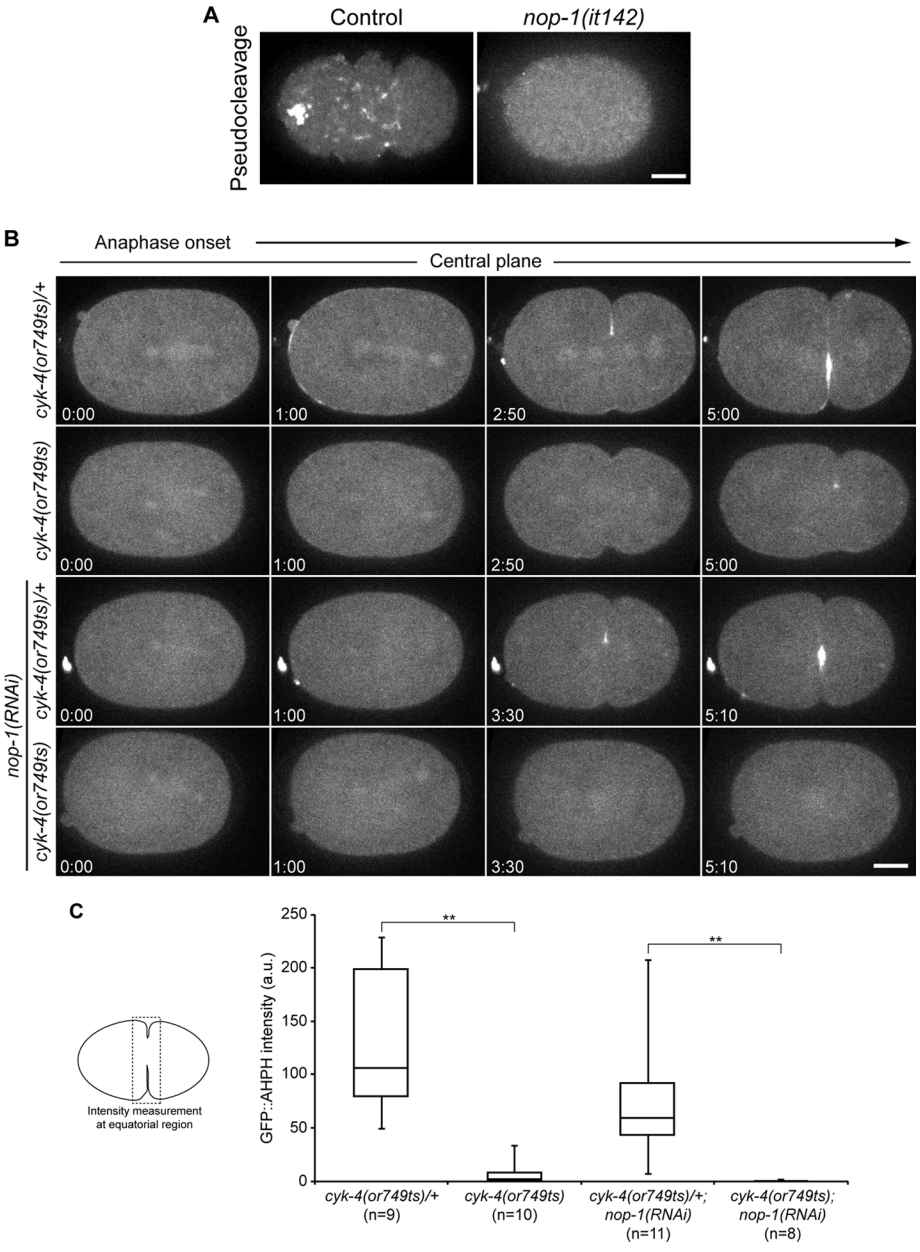

FIGURE 5: CYK-4 and NOP-1 regulate the recruitment of the active RhoA biosensor. (A) Confocal images of cortical planes of control and *nop-1(it142)* embryos expressing GFP::AHPH during pseudocleavage. (B) Selected confocal images from central planes from time-lapse sequences of *cyk-4(or749ts)/+*, *cyk-4(or749ts)*, *cyk-4(or749ts)/+;nop-1(RNAi)*, and *cyk-4(or749ts);nop-1(RNAi)* embryos expressing GFP::AHPH. (C) Box-and-whisker plot of the equatorial accumulation of GFP::AHPH of embryos as shown in (A). **, $p < 0.01$.

NOP-1 regulates polarity establishment

As polarity is established, cortical myosin flows away from the sperm microtubule organizing center to the opposite pole, where it forms an anterior cap enriched in large myosin foci. This cortical flow of myosin promotes the concurrent flow of PAR-6/PAR-3/PKC-3 and its accumulation at the anterior pole (Munro *et al.*, 2004). In NOP-1–depleted embryos, the cortical flow of myosin is weaker, and the assembly of large myosin patches in the anterior is abolished (Figure 7A). A significant subset of *nop-1(it142)* embryos lacked cortical flows altogether (11/56); these embryos exhibited a high incidence of symmetric or failed first division (7/11 and 4/11, respectively), and all of these embryos failed to hatch. These results suggest that *nop-1* is a *Par* gene with incomplete penetrance. Consistent with reduced cortical flows, the anterior cap of myosin occupies ~65% of egg length in *nop-1(it142)* embryos, as compared with ~52% in control embryos (Figure 7B), indicating that loss of NOP-1 is sufficient to impair polarization. Although cortical flows persist in *par-2*(*RNAi*) embryos (Munro *et al.*, 2004), microtubule-directed localization of PAR-2 can establish polarity in embryos defective in RhoA activation (Zonies *et al.*, 2010; Motegi *et al.*, 2011). Depletion of PAR-2 eliminated the residual polarization observed in *nop-1(it142)* embryos (Figure 7A), analogous to the previously demonstrated redundancy between PAR-2 and ECT-2 (Zonies *et al.*, 2010).

To gain further insight into the mechanism by which NOP-1 promotes embryo polarization, we investigated whether NOP-1 regulates the dynamics of PAR protein accumulation. We imaged embryos coexpressing mCherry::PAR-6 and GFP::PAR-2 in control and NOP-1–depleted embryos. In control embryos, mCherry::PAR-6 initially occupies the entire cortex near the end of meiosis. As PAR-6 begins to recede from the posterior pole, GFP::PAR-2 is recruited to the cortex at the posterior, and the PAR-2-PAR-6 boundary shifts anteriorly until both domains occupy ~50% of the length of the

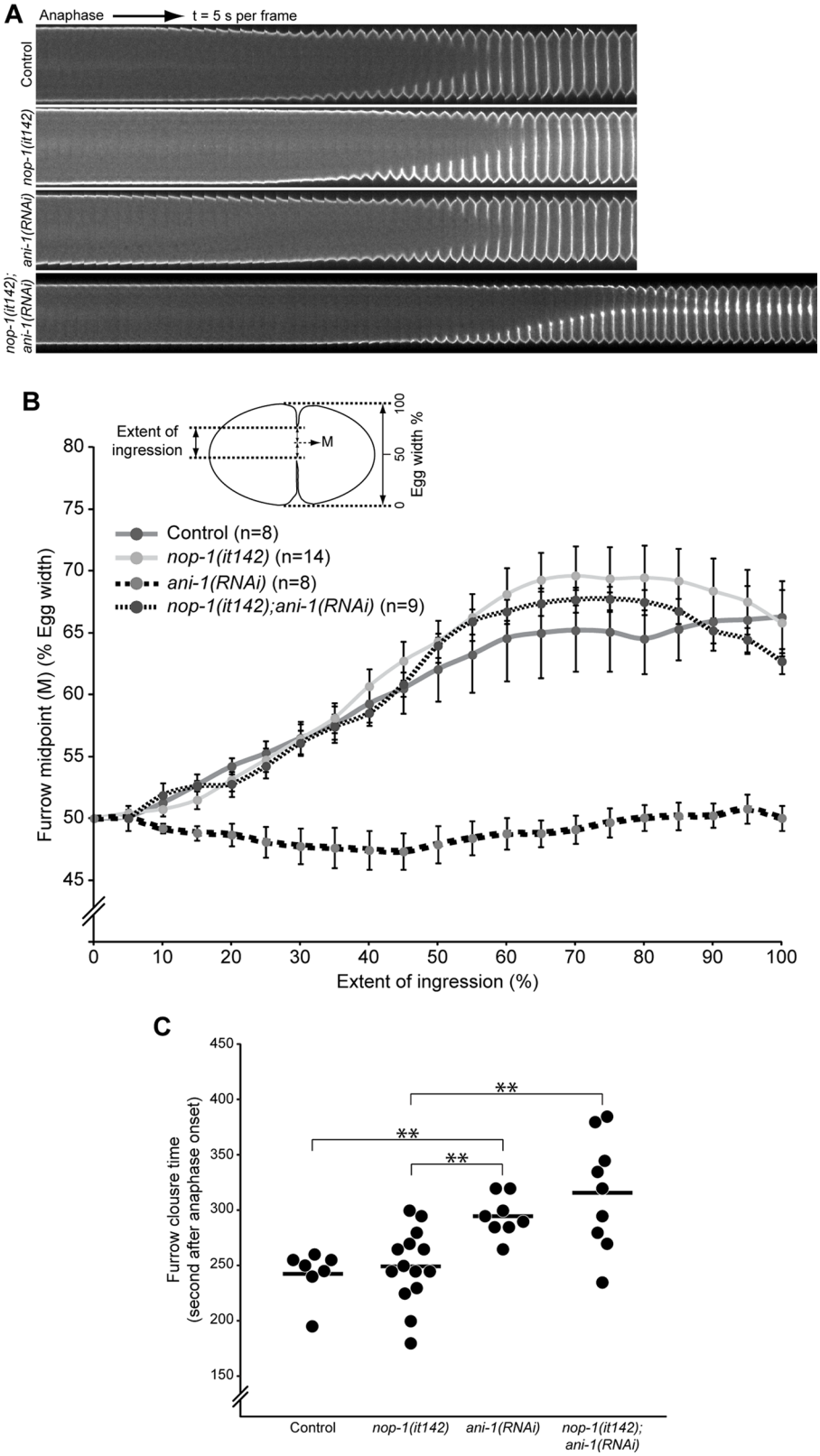

FIGURE 6: NOP-1 and ANI-1 are dispensable for asymmetric cleavage furrow ingression. (A) Kymograph of equatorial segments of control, *nop-1(it142)*, *ani-1(RNAi)*, and *nop-1(it142);ani-1(RNAi)* embryos expressing a plasma membrane marker, GFP::PH, from anaphase onset. Images were acquired at 5-s intervals. (B) Position of the midpoint (M) between the two furrow tips expressed as percent egg width as a function of the extent of furrow ingression of embryos acquired as in (A). (C) Time required for complete furrow ingression as determined from time-lapse sequences acquired as in (A). Error bars represent ± SEM; **, $p < 0.01$.

embryo. Recruitment of GFP::PAR-2 occurs around 600 s before nuclear envelope breakdown (NEBD) in control embryos (Figure 7, C and D). GFP::PAR-2 recruitment is delayed by ~150 s in *nop-1(it142)* embryos and *nop-1(RNAi)* embryos, occurring ~450 s before NEBD (Figure 7, C and D). A similar delay in symmetry breaking has been reported in *ect-2(ax751ts)* embryos (Zonies *et al.*, 2010). Indeed, both hypomorphic, temperature-sensitive *ect-2(ax751ts)* embryos and *ect-2(RNAi)* embryos recruit GFP::PAR-2 ~400 s before NEBD (Figure 7, C and D). GFP::PAR-2 recruitment is further delayed to ~200 s before NEBD in *ect-2(ax751ts);ect-2(RNAi)* embryos. Likewise, PAR-2 recruitment is significantly delayed in *nop-1(it142);ect-2(RNAi)* embryos and *ect-2(ax751ts);nop-1(RNAi)* embryos, as compared with the single mutants (Figure 7, C and D). Thus the residual ECT-2 activity in *ect-2(RNAi)* embryos and in *ect-2(ax751ts)* embryos requires NOP-1. Intriguingly, the strong inactivation of ECT-2 by depletion of the mutant protein delays polarization more strongly than mutational inactivation of NOP-1, raising the possibility of trace ECT-2 activity in the absence of NOP-1.

DISCUSSION

We have demonstrated that both polarization and cytokinesis involve a protein, NOP-1, that promotes the characteristic events downstream of RhoA activation. NOP-1 is critical for these events during polarization. During cytokinesis, NOP-1 makes a significant contribution to these processes, but the centralspindlin subunit CYK-4 plays the dominant role in promoting RhoA-dependent events. Due to redundant pathways for polarization and cytokinesis, the majority of *nop-1* embryos successfully polarize and divide, despite significant molecular defects.

NOP-1 is an unusual protein. It is serine-rich and lacks obvious conserved domains and orthologues outside the *Caenorhabditis* genus. Interestingly, pseudocleavage is observed in embryos of many, but not all, species within the Rhabditidae family (Brauchle *et al.*, 2009). The absence of molecular clues creates challenges for the elucidation of NOP-1's function. However, thorough phenotypic characterization indicates that NOP-1 is required for the cortical recruitment of myosin and anillin and the proper organization of F-actin during the establishment phase of polarization and during central spindle–independent cytokinesis (Figure 8A). Cortical accumulation of these RhoA effectors are largely independent of each other. Furthermore, NOP-1 promotes cortical recruitment of a RhoA biosensor.

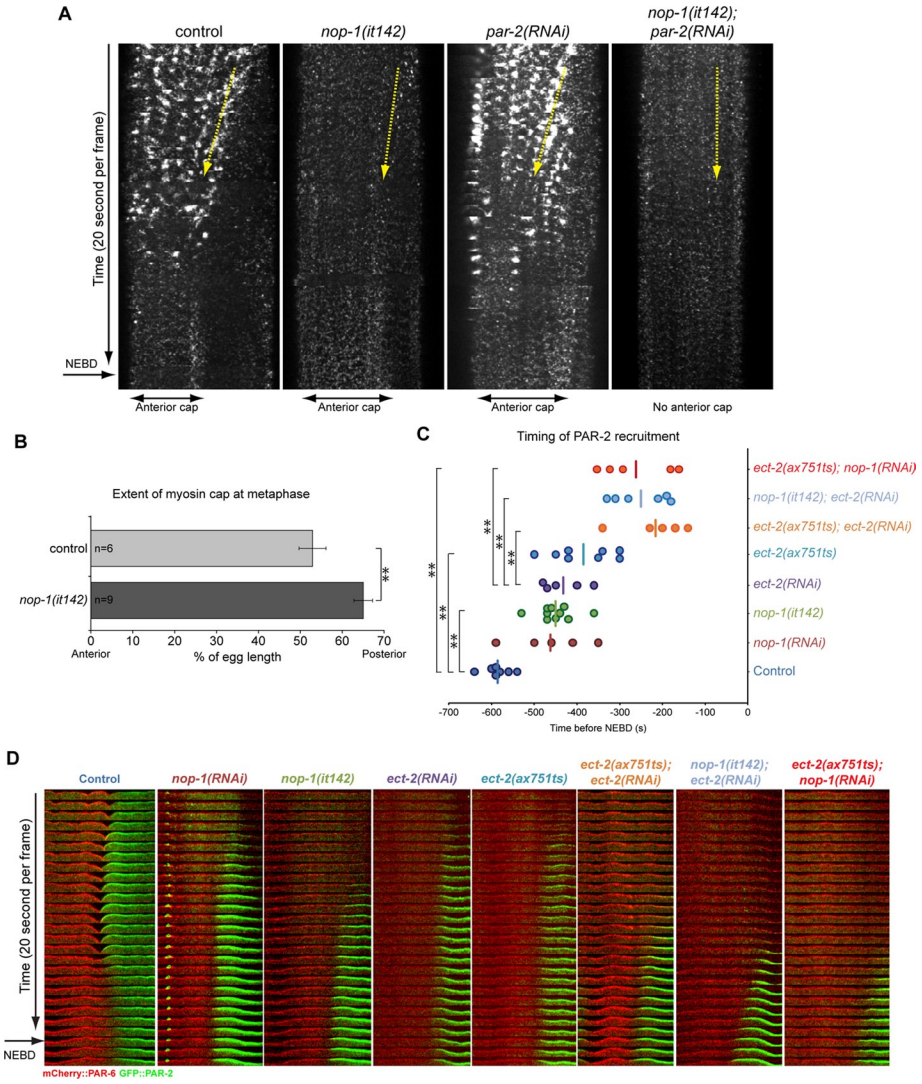

FIGURE 7: NOP-1 regulates polarity establishment. (A) Kymographs of a cortical slice along the AP-axis of control, *nop-1(it142)*, *par-2(RNAi)*, and *nop-1(it142);par-2(RNAi)* embryos expressing NMY-2::GFP prior to NEBD. The yellow arrow indicates the direction of cortical flow of myosin. (B) Quantification of the size of the metaphase cap of NMY-2::GFP in control and *nop-1(it142)* embryos. (C) Quantification of the timing of cortical recruitment of GFP::PAR-2 in control, *nop-1(RNAi)*, *nop-1(it142)*, *ect-2(RNAi)*, *ect-2(ax751ts)*, *ect-2(ax751ts);ect-2(RNAi)*, *ect-2(ax751ts);nop-1(RNAi)*, and *nop-1(it142);ect-2(RNAi)* embryos expressing GFP::PAR-2 and mCherry::PAR-6. Each filled circle represents an individual embryo, and the straight lines represent the average time of recruitment. **, $p < 0.01$. (D) Kymograph of the segment across the AP-axis of embryos in (C) prior to NEBD.

Therefore NOP-1 is not likely to mediate the biosynthesis or recruitment of one effector and indirectly inhibit recruitment of the other effectors. More likely, NOP-1 acts upstream of these components by promoting accumulation of active RhoA (Figure 8B). In principle, it could do so by inhibiting an inhibitor of RhoA. However, NOP-1 is required for cortical contractility in embryos depleted of a Rho family GAP, RGA-3/4, which acts antagonistically to ECT-2, formally ruling out the possibility that NOP-1 is an inhibitor of this RhoGAP. NOP-1 is also required for contractility in *rfl-1* embryos, another condition that would favor accumulation of active RhoA. Thus we favor the hypothesis that NOP-1 promotes RhoA activation. The factors known to promote RhoA activation include the RhoGEF ECT-2 and the RhoGAP CYK-4. Whereas ECT-2 is required for all RhoA activity in the embryo, NOP-1 and CYK-4 promote separable aspects of RhoA function. As NOP-1 function in the embryo requires ECT-2, it must function upstream of ECT-2.

How might NOP-1 promote RhoA activation? There are indications of ECT-2 autoinhibition. The N- and C-termini of ECT-2 interact, and mutations in the N-terminus can activate aspects of ECT-2 function (Kim *et al.*, 2005). During cytokinesis in human cells, direct binding of CYK-4 to ECT-2 is required for ECT-2 activity, and this may relieve ECT-2's autoinhibition (Yüce *et al.*, 2005; Burkard *et al.*, 2009; Wolfe *et al.*, 2009). Interestingly, the GAP domain of CYK-4 also contributes to full activation of ECT-2. Although CYK-4 and NOP-1 are not detectably related, a phosphorylated form of NOP-1 might interact with the tandem BRCT domains of ECT-2, as is the case for CYK-4 (Wolfe *et al.*, 2009).

NOP-1 is required for RhoA-dependent contractility events during polarization. In contrast, *cyk-4(or749ts)* embryos, which contain a substitution mutation in the GAP domain, do not have a detectable phenotype during polarity establishment. Although sperm-derived CYK-4 was proposed to promote polarization in the early embryo through local RhoA-GAP activity at the embryonic posterior (Jenkins *et al.*, 2006), this proposal is not consistent with observations in *cyk-4(or749ts)* embryos, nor has it not garnered additional experimental support.

During cytokinesis, RhoA activation relies on both NOP-1 and CYK-4. In *nop-1* embryos, the vast majority of RhoA-dependent processes require CYK-4 and vice versa. These results suggest that NOP-1 and CYK-4 are parallel activators of ECT-2 during cytokinesis, with CYK-4 playing a quantitatively dominant role. Indeed, cytokinesis can proceed to completion in *nop-1* embryos, but furrow ingression is incomplete in *cyk-4* embryos (Jantsch-Plunger *et al.*, 2000).

Furrow formation during cytokinesis involves both astral microtubules and the central spindle. CYK-4 is required for central spindle–directed furrowing and NOP-1 is primarily involved in aster-induced furrowing. Previous studies (Werner *et al.*, 2007), have shown that central spindle–directed accumulation of RhoA effectors is highly localized. In contrast, central spindle–independent accumulation of RhoA effectors, shown here to require NOP-1, is largely dispersed (Figure 8C). Microtubules and anillin function together to focus these dispersed effectors (Tse *et al.*, 2011).

Depletion of a number of proteins can prevent furrowing in central spindle–defective embryos. This list includes factors that promote spindle elongation (GOA-1 and GPA-16, GPR-1/2, LET-99), factors that promote myosin organization (ANI-1), and factors that promote myosin contractility (protein phosphatase 6, PPH-6, and its associated subunit SAPS-1). When spindle elongation is perturbed in central spindle–deficient embryos, cortical myosin

accumulates, but it is not sufficiently polarized to allow formation of a ingressing furrow (Dechant and Glotzer, 2003; Bringmann *et al.*, 2007; Werner *et al.*, 2007). When ANI-1 is depleted, myosin accumulates on the cortex, but it is not organized into large foci, nor is the myosin highly polarized, again preventing furrow formation in central spindle–defective embryos (Tse *et al.*, 2011). Depletion of PPH-6 or SAPS-1 also allows myosin accumulation (Afshar *et al.*, 2010), although it is less contractile, perhaps due to a failure in Aurora A activation (Zeng *et al.*, 2010). Thus, in each of these cases, there is significant cortical recruitment of RHO-1 effectors, creating the potential for aster-dependent contractility. NOP-1 is distinct from these factors in that its inactivation in central spindle–deficient embryos abrogates recruitment of cortical myosin II and anillin. Thus NOP-1 depletion is the most stringent means available to inhibit aster-directed furrowing without greatly compromising central spindle–directed furrowing.

In wild-type *C. elegans* embryos, the cleavage furrow ingresses asymmetrically. Asymmetric furrow ingression is observed in a variety of cell types, but its mechanistic basis is not understood. Asymmetric ingression requires anillin and septins, and it is associated with increased myosin recruitment at the rapidly ingressing side of the furrow (Maddox *et al.*, 2007). The trigger for symmetry breaking is not known. One proposal involves a positive feedback loop in which contractile proteins recruit anillin, which promotes increased accumulation of contractile proteins (Maddox *et al.*, 2007). Unexpectedly, we have found that embryos deficient in both NOP-1 and anillin have asymmetrically ingressing cleavage furrows. Thus there are anillin-independent mechanisms that lead to furrow asymmetry. From a genetic perspective, a corollary of these findings is that NOP-1 prevents asymmetric furrow formation in ANI-1–deficient embryos. Furrow formation in embryos deficient in both NOP-1 and anillin is entirely due to centralspindlin–dependent activation of RhoA. One explanation of these results could be that central spindle–directed furrowing is intrinsically asymmetric, perhaps due to the effect of spindle oscillations on the proximity of the central spindle to the cortex. When anillin is absent, NOP-1–dependent cortical accumulation of RhoA effectors may antagonize the asymmetric furrowing induced by the central spindle pathway. However, other explanations are also viable, and additional analysis of the mechanisms governing recruitment of contractile proteins is required to more deeply understand the mechanics of cleavage furrow ingression.

NOP-1 is not only an important, nonessential regulator of cytokinesis, it is also an important, nonessential regulator of cell polarization. The molecular function of NOP-1 in these two processes appears similar, namely, promoting RhoA activation. Polarization is known to involve RhoA and ECT-2. A mutation in *ect-2*, *ax751ts*, causes a phenotype similar to that seen with mutations in *nop-1* (Zonies *et al.*, 2010). This allele of *ect-2* is hypomorphic; further depletion of ECT-2 by RNAi or inactivation of NOP-1 strengthens the phenotype, consistent with the model that NOP-1 is an activator of ECT-2. Indeed, both *nop-1(it142)* and *ect-2(ax751ts)* delay embryo polarity establishment and the combination of either mutation with depletion of PAR-2 abrogates embryo polarization (this paper and Zonies *et al.*, 2010). These results demonstrate that NOP-1 functions in a RhoA-dependent pathway for embryo polarization that acts in parallel to a PAR-2–dependent pathway.

Collectively our results indicate that NOP-1 serves as a second upstream activator of the RhoA GEF, ECT-2, acting in parallel with CYK-4. These two activators are not simply redundant. During polarization, CYK-4 appears largely inactive and NOP-1 is required for the majority of RhoA-dependent events. During cytokinesis, both activators are active, but they appear to function at different sites, as

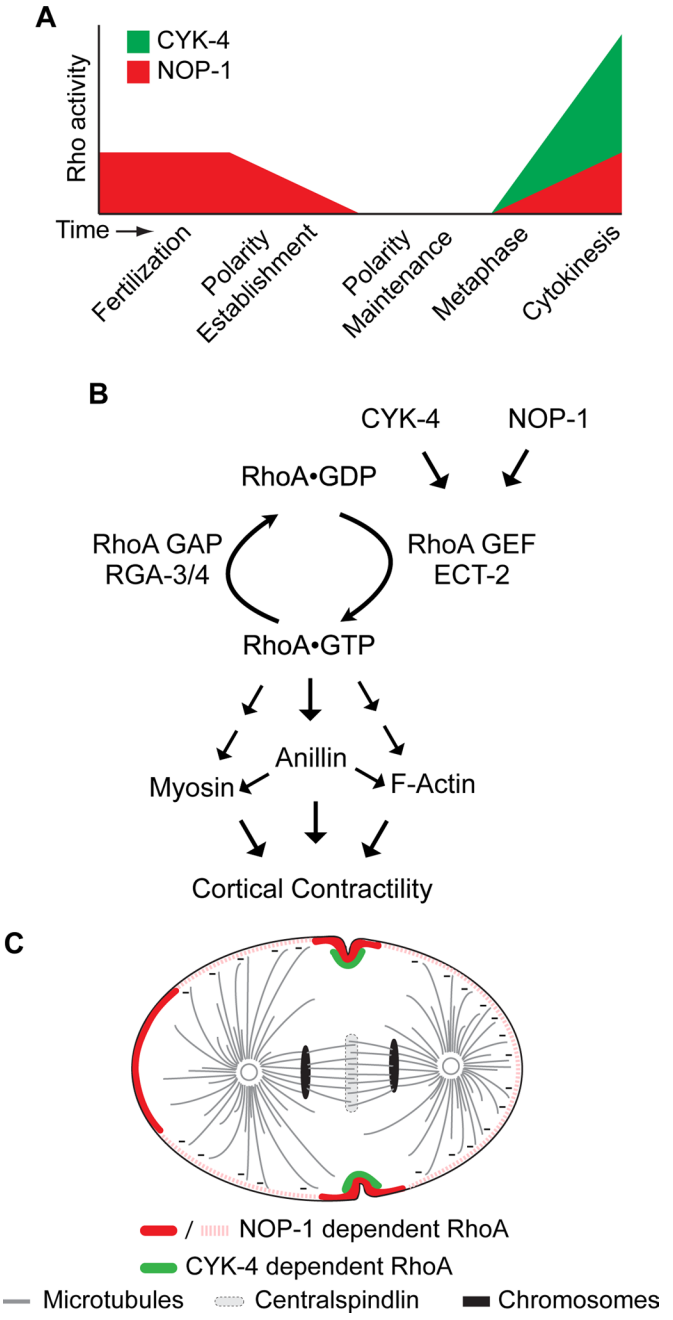

FIGURE 8: (A) Summary depicting the kinetics of RhoA activation during the first division of the early *C. elegans* embryo, roughly indicating the relative contributions of NOP-1 (red) and CYK-4 (green). (B) The pathway by which RhoA and its effectors are activated during cytokinesis. (C) Schematic of cytokinesis of an early *C. elegans* embryo depicting the local, CYK-4–dependent activation of RhoA (green) and the more dispersed accumulation dependent on NOP-1 (red).

CYK-4 is largely restricted to the central spindle. During both polarization and cytokinesis, NOP-1 may serve as a global activator of RhoA subject to aster- and centrosome-dependent modulation.

MATERIALS AND METHODS

Strains

C. elegans strains (listed in Table S1) were maintained on nematode growth medium (NGM) plates using standard procedures. Unless otherwise specified, strains were provided by the Caenorhabditis

Genetics Center, which is funded by the National Institutes of Health (NIH) National Center for Research Resources.

RNAi

Generally, RNAi was administered by feeding nematodes with *Escherichia coli* expressing the appropriate double-stranded RNA (dsRNA; Timmons and Fire, 1998). HT115 bacterial cultures were grown in Luria broth with 100 μg/ml ampicillin overnight at 37°C. Cultures (200 μl) were seeded on NGM plates containing 100 μg/ml ampicillin and 1 mM isopropyl β-D-1-thiogalactopyranoside and incubated at room temperature (~23°C) for 8 h. RNAi plasmids were obtained from the library produced by Kamath *et al.* (2003). Young L4 hermaphrodites were picked onto the plates for feeding at 25°C at least 24 h prior to dissection. The one exception to this was for Supplemental Figure S5, for which ECT-2 was depleted by injection of in vitro synthesized dsRNA. In this case, analysis was restricted to embryos that exhibited no furrowing in either the first or the second division.

Mapping of *nop-1*

nop-1 was previously mapped to the region of chromosome III between *dpy-17* and unc-32 (Rose *et al.*, 1995). Deficiency mapping placed *nop-1* in the 0.06 cM region between the deficiencies *sDf121* and *sDf127*. For further refinement of the mapping, *lon-1(e185);nop-1(it42);unc-36(e251)/qC1* animals were crossed with *unc-32(e189);cyk-3(t1525);sma-4(e729)/qC1* animals. We picked 111 recombinants that separated *sma-4* and unc-32. Thirteen recombinants' lines produced viable progeny, indicating that the recombination event took place between *sma-4* and *cyk-3*. We performed time-lapse Nomarski imaging of at least 10 embryos from these 13 lines. Seven lines produced some embryos with pseudocleavage defects, positioning *nop-1* approximately midway between *sma-4* and *cyk-3*. We then used RNAi to the genes in this specific region to identify the gene, F25B5.2, whose depletion phenocopies *nop-1(it42)*.

Transgenic lines

Transgenic lines expressing GFP::NOP-1, GFP::Utrophin, and GFP::AHPH were integrated into the Mos element ttTi5605 on chromosome II using the MosSCI method (Frøkjaer-Jensen *et al.*, 2008).

Microscopy

Gravid hermaphrodites were dissected in egg salt buffer on coverslips, mounted on 2.5% agarose pads, and sealed with Vaseline. For Nomarski imaging, embryos were observed with a Zeiss (Thornwood, NY) Axioplan II with a 100×/1.3 Plan-Neofluar objective. Images were captured with a charge-coupled device (CCD) camera (Imaging Source, Charlotte, NC) controlled by Gawker (http://gawker.sourceforge.net). Images were acquired every 5 s and processed with ImageJ (http://rsbweb.nih.gov/ij). For confocal imaging, embryos were imaged with a 63×/1.4 numerical aperture oil-immersion lens on 1) a Zeiss Axiovert 200M equipped with a Yokogawa CSU-10 spinning-disk unit (McBain, Simi Valley, CA) and illuminated with 50-mW, 473-nm and 20-mW, 561-nm lasers (Cobolt, Solna, Sweden), or 2) a Zeiss Axioimager M1 equipped with a Yokogawa CSU-X1 spinning-disk unit (Solamere, Salt Lake City, UT) and illuminated with 50-mW, 488-nm and 50-mW, 561-nm lasers (Coherent, Santa Clara, CA). Images were captured on a Cascade 1K EM-CCD camera or a Cascade 512BT (Photometrics, Tucson, AZ) controlled by MetaMorph (Molecular Devices, Sunnyvale, CA). Image processing was performed with ImageJ. Z-stacks were projected with a maximum-intensity algorithm. Time-lapse projections were assembled into movies using MetaMorph and ImageJ. *cyk-4(or749ts)* embryos were imaged with an objective heater, all other images, including *ect-2(ax751ts)*, were acquired at room temperature ~23°C.

Image quantification

For measurement of the kinetics of membrane ingression, montages produced from embryos expressing the plasma membrane marker GFP::PH were opened in ImageJ, and the tips of the membrane ingression were manually positioned. The coordinates were then imported into Excel for further analysis. The maximum length of myosin cap and the timing of GFP::PAR-2 recruitment were manually analyzed in ImageJ. To quantify the accumulation of GFP::AHPH at the furrow region, we measured the intensity of pixels that exceeded a threshold of 1.45 × background for each slice. To quantify the accumulation of GFP::NMY-2 and GFP::ANI-1 in the entire cortex, we measured the intensity of pixels that exceeded a threshold of 1.45 × background for each slice. To quantify the changes of GFP::Utrophin, we measured the average intensity in a 30-pixel-wide region at 50–75% egg length.

ACKNOWLEDGMENTS

This work was supported by an NIH grant (R01GM085087) to M.G. and an American Heart Association Midwest Postdoctoral Fellowship (#09POST2110164) to Y.C.T. We thank Ed Munro and Geraldine Seydoux for helpful discussions related to this work.

REFERENCES

Afshar K, Werner ME, Tse YC, Glotzer M, Gönczy P (2010). Regulation of cortical contractility and spindle positioning by the protein phosphatase 6 PPH-6 in one-cell stage *C. elegans* embryos. Development 137, 237–247.

Brauchle M, Kiontke K, MacMenamin P, Fitch DHA, Piano F (2009). Evolution of early embryogenesis in rhabditid nematodes. Dev Biol 335, 253–262.

Bringmann H, Cowan CR, Kong J, Hyman AA (2007). LET-99, GOA-1/GPA-16, and GPR-1/2 are required for aster-positioned cytokinesis. Curr Biol 17, 185–191.

Bringmann H, Hyman AA (2005). A cytokinesis furrow is positioned by two consecutive signals. Nature 436, 731–734.

Burkard ME *et al.* (2009). Plk1 self-organization and priming phosphorylation of HsCYK-4 at the spindle midzone regulate the onset of division in human cells. PLoS Biol 7, e1000111.

Burkel BM, Dassow von G, Bement WM (2007). Versatile fluorescent probes for actin filaments based on the actin-binding domain of utrophin. Cell Motil Cytoskeleton 64, 822–832.

Canman JC, Lewellyn L, Laband K, Smerdon SJ, Desai A, Bowerman B, Oegema K (2008). Inhibition of Rac by the GAP activity of centralspindlin is essential for cytokinesis. Science 322, 1543–1546.

Cowan CR, Hyman AA (2004). Centrosomes direct cell polarity independently of microtubule assembly in *C. elegans* embryos. Nature 431, 92–96.

Cuenca AA, Schetter A, Aceto D, Kemphues K, Seydoux G (2003). Polarization of the *C. elegans* zygote proceeds via distinct establishment and maintenance phases. Development 130, 1255–1265.

Dechant R, Glotzer M (2003). Centrosome separation and central spindle assembly act in redundant pathways that regulate microtubule density and trigger cleavage furrow formation. Dev Cell 4, 333–344.

Frøkjaer-Jensen C, Davis MW, Hopkins CE, Newman BJ, Thummel JM, Olesen S-P, Grunnet M, Jorgensen EM (2008). Single-copy insertion of transgenes in *Caenorhabditis elegans*. Nat Genet 40, 1375–1383.

Gotta M, Abraham MC, Ahringer J (2001). CDC-42 controls early cell polarity and spindle orientation in *C. elegans*. Curr Biol 11, 482–488.

Jantsch-Plunger V, Gönczy P, Romano A, Schnabel H, Hamill D, Schnabel R, Hyman AA, Glotzer M (2000). CYK-4: A Rho family GTPase activating protein (GAP) required for central spindle formation and cytokinesis. J Cell Biol 149, 1391–1404.

Jenkins N, Saam JR, Mango SE (2006). CYK-4/GAP provides a localized cue to initiate anteroposterior polarity upon fertilization. Science 313, 1298–1301.

Kamath RS *et al.* (2003). Systematic functional analysis of the *Caenorhabditis elegans* genome using RNAi. Nature 421, 231–237.

Kay AJ, Hunter CP (2001). CDC-42 regulates PAR protein localization and function to control cellular and embryonic polarity in *C. elegans*. Curr Biol 11, 474–481.
Kim J-E, Billadeau DD, Chen J (2005). The tandem BRCT domains of Ect2 are required for both negative and positive regulation of Ect2 in cytokinesis. J Biol Chem 280, 5733–5739.
Kumfer KT, Cook SJ, Squirrell JM, Eliceiri KW, Peel N, O'Connell KF, White JG (2010). CGEF-1 and CHIN-1 regulate CDC-42 activity during asymmetric division in the *Caenorhabditis elegans* embryo. Mol Biol Cell 21, 266–277.
Loria A, Longhini KM, Glotzer M (2012). The RhoGAP domain of CYK-4 has an essential role in RhoA activation. Curr Biol 22, 213–219.
Maddox AS, Habermann B, Desai A, Oegema K (2005). Distinct roles for two *C. elegans* anillins in the gonad and early embryo. Development 132, 2837–2848.
Maddox AS, Lewellyn L, Desai A, Oegema K (2007). Anillin and the septins promote asymmetric ingression of the cytokinetic furrow. Dev Cell 12, 827–835.
Motegi F, Sugimoto A (2006). Sequential functioning of the ECT-2 RhoGEF, RHO-1 and CDC-42 establishes cell polarity in *Caenorhabditis elegans* embryos. Nat Cell Biol 8, 978–985.
Motegi F, Zonies S, Hao Y, Cuenca AA, Griffin E, Seydoux G (2011). Microtubules induce self-organization of polarized PAR domains in *Caenorhabditis elegans* zygotes. Nat Cell Biol 13, 1361–1367.
Munro E, Bowerman B (2009). Cellular symmetry breaking during *Caenorhabditis elegans* development. Cold Spring Harb Perspect Biol 1, a003400.
Munro E, Nance J, Priess JR (2004). Cortical flows powered by asymmetrical contraction transport PAR proteins to establish and maintain anterior-posterior polarity in the early *C. elegans* embryo. Dev Cell 7, 413–424.
Piekny A, Werner M, Glotzer M (2005). Cytokinesis: welcome to the Rho zone. Trends Cell Biol 15, 651–658.
Piekny AJ, Glotzer M (2008). Anillin is a scaffold protein that links RhoA, actin, and myosin during cytokinesis. Curr Biol 18, 30–36.
Rose LS, Lamb ML, Hird SN, Kemphues KJ (1995). Pseudocleavage is dispensable for polarity and development in *C. elegans* embryos. Dev Biol 168, 479–489.
Schmutz C, Stevens J, Spang A (2007). Functions of the novel RhoGAP proteins RGA-3 and RGA-4 in the germ line and in the early embryo of *C. elegans*. Development 134, 3495–3505.
Schonegg S, Constantinescu AT, Hoege C, Hyman AA (2007). The Rho GTPase-activating proteins RGA-3 and RGA-4 are required to set the initial size of PAR domains in *Caenorhabditis elegans* one-cell embryos. Proc Natl Acad Sci USA 104, 14976–14981.
Schonegg S, Hyman AA (2006). CDC-42 and RHO-1 coordinate acto-myosin contractility and PAR protein localization during polarity establishment in *C. elegans* embryos. Development 133, 3507–3516.
Timmons L, Fire A (1998). Specific interference by ingested dsRNA. Nature 395, 854.
Tsai MC, Ahringer J (2007). Microtubules are involved in anterior-posterior axis formation in *C. elegans* embryos. J Cell Biol 179, 397–402.
Tse YC, Piekny A, Glotzer M (2011). Anillin promotes astral microtubule-directed cortical myosin polarization. Mol Biol Cell 22, 3165–3175.
Werner M, Glotzer M (2008). Control of cortical contractility during cytokinesis. Biochem Soc Trans 36, 371–377.
Werner M, Munro E, Glotzer M (2007). Astral signals spatially bias cortical myosin recruitment to break symmetry and promote cytokinesis. Curr Biol 17, 1286–1297.
Wolfe BA, Takaki T, Petronczki M, Glotzer M (2009). Polo-like kinase 1 directs assembly of the HsCyk-4 RhoGAP/Ect2 RhoGEF complex to initiate cleavage furrow formation. PLoS Biol 7, e1000110.
Yamada T, Hikida M, Kurosaki T (2006). Regulation of cytokinesis by mgcRacGAP in B lymphocytes is independent of GAP activity. Exp Cell Res 312, 3517–3525.
Yüce O, Piekny A, Glotzer M (2005). An ECT2-centralspindlin complex regulates the localization and function of RhoA. J Cell Biol 170, 571–582.
Zeng K, Bastos RN, Barr FA, Gruneberg U (2010). Protein phosphatase 6 regulates mitotic spindle formation by controlling the T-loop phosphorylation state of Aurora A bound to its activator TPX2. J Cell Biol 191, 1315–1332.
Zonies S, Motegi F, Hao Y, Seydoux G (2010). Symmetry breaking and polarization of the *C. elegans* zygote by the polarity protein PAR-2. Development 137, 1669–1677.